

Supplementary information
Catalytic activation of peroxymonosulfate by Mn/N co-
doped porous carbon for effective phenol degradation:
Crucial role of non-radical pathways

*Qi Guo^a, Jihong Xu^a, Rui Tang^{a, b, *}, Yulin Min^{a, b}, Zhenhu Hu^c, Penghui Shi^{a, b, *}*

^a Shanghai Key Laboratory of Materials Protection and Advanced Materials in Electric Power, Shanghai University of Electric Power, Shanghai 200090, P. R. China

^b Shanghai Institute of Pollution Control and Ecological Security, Shanghai 200090, P. R. China

^c Anhui Engineering Laboratory of Rural Water Environment and Resource, School of Civil Engineering, Hefei University of Technology, Hefei 230009, P. R. China

* Corresponding author. Tel.: +86 18801618059; E-mail addresses:
tangrui@shiep.edu.cn (R. Tang), shipenghui@shiep.edu.cn (P. Shi).

Contents

Text S1. Electrochemical measurements

Text S2. Determination of Reactive Species

Text S3. Selective oxidation in Mn-N@C-1/PMS system

Table S1. Physicochemical properties of target contaminants.

Table S2. HPLC conditions for the analysis of target contaminants.

Table S3. Second-order rate constants ($M^{-1} s^{-1}$) between radicals and probe compounds.

Table S4. The surface chemistry of Fresh/Used Mn-N@C-1 according to XPS results.

Table S5. The chemical compositions of Fresh/Used Mn-N@C-1 according to XPS results.

Table S6. Characteristics of SW and ST samples.

Fig. S1. N_2 adsorption–desorption isotherms of N@C and Mn-N@C-1

Fig. S2. TEM images of Mn-N@C-2.

Fig. S3. TEM images of Mn@C.

Fig. S4. XRD patterns of N@C, Mn@CN, and Mn-N@C-1

Fig. S5. (a) Phenol adsorption and oxidation of Mn-N@C-1; (b) Pseudo-first-order kinetic fitting of Mn-N@C-1 on phenol degradation.

Fig. S6. Phenol oxidation of Mn@CN and Mn-N@C-1.

Fig. S7. Zeta potential of Mn-N@C-1.

Fig. S8. Phenol degradation in Mn-N@C-1/PMS system under different Mn-N@C-1 dosage.

Fig. S9. Phenol degradation in Mn-N@C-1/PMS system under different PMS dosage.

Fig. S10. The Mn leaching concentration after successive runs of phenol oxidation

Fig. S11. Phenol degradation via PMS activation using Mn^{2+} catalyst.

Fig. S12. EPR spectra of $^1\text{O}_2$ detection in the presence of TEMP and BQ.

Fig. S13. (a) Selective oxidation in Mn-N@C-1/PMS system; (b) Pseudo-first-order kinetic fitting of selective oxidation in Mn-N@C-1/PMS system.

Text S1. Electrochemical measurements

First, a catalyst-supported carbon paper electrode was prepared. Nafion solution (5.0 wt % isopropanol in water) and catalyst powder (20 mg) were sonicated with ethanol (2 ml) for 4 hours. The mixed suspension was dropped onto the surface of a carbon paper electrode. The carbon paper electrode was vacuum-dried at 60°C for 8 hours. Install the standard three-electrode configuration, with carbon paper electrodes as working electrodes, Pt electrodes as counter electrodes, and Ag/AgCl (4 M KCl) as reference electrodes. The battery reactor contains 0.5 M Na₂SO₄ electrolyte. Electrochemical measurements were performed by the CHI 760E instrument (Shanghai Chenhua Instrument Company, China). LSV was performed in the potential region from -1 to -0.2 V (vs. Ag/AgCl) at a scan rate of 10 mV s⁻¹. EIS was measured under a frequency range of 1 Hz-100 kHz with 5 mV amplitude.

Text S2. Determination of Reactive Species

EPR spectra were recorded on a Bruker A300 spectrometer at 25°C to investigate the ROS generating from the Mn-N@C-1/PMS system. 5,5-dimethyl-1-pyrroline N-oxide (DMPO, > 97%, Aladdin) and 2,2,6,6-tetramethyl-4-piperidinol (TEMP, GC, Aladdin) were employed as spin trapping agents to capture reactive species. Specifically, 0.5 mL sample was withdrawn from Mn-N@C-1/PMS system in 3 min and filtered through a 0.22 μm membrane. Then, 0.35 M DMPO or TEMP solution (200 μL) was mixed with 200 μL filtered sample. Finally, using a quartz capillary to absorb the mixed solution, followed by using an EPR spectrometer to detect the corresponding signal.

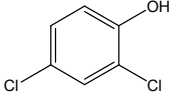
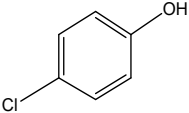
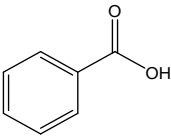
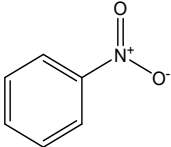
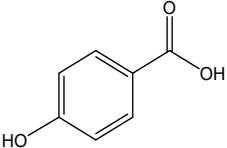
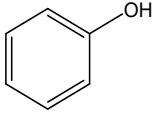
Text S3. Selective oxidation in Mn-N@C-1/PMS system

As shown in Fig. S13a, the oxidative degradation of 4-CP, BPA, 2,4-DCP, and phenol was effective. Their k_{obs} values were calculated to be 0.242 min^{-1} , 0.470 min^{-1} , 1.043 min^{-1} , and 1.122 min^{-1} in the Mn-N@C-1/PMS system (Fig. S13b), respectively, and the removal effect was remarkable. While k_{obs} values of BA and NB were 0.007 min^{-1} and 0.016 min^{-1} , which were hardly removed, indicating that the Mn-N@C-1/PMS system was selective in the pollutant oxidation process. In addition, BA acted as the indicating probe for $\text{SO}_4^{\bullet-}$ and $\bullet\text{OH}$ ($k(\text{BA}, \bullet\text{OH}) = 4.2 \times 10^9 \text{ M}^{-1} \text{ s}^{-1}$ and $k(\text{BA}, \text{SO}_4^{\bullet-}) = 1.2 \times 10^9 \text{ M}^{-1} \text{ s}^{-1}$).¹ Its degradation rate was almost zero, indicating that the free radical pathway was not involved in the reaction process, which was consistent with the quenching experimental results. Therefore, the activation mechanism of PMS could be inferred according to the selective oxidation of pollutants by Mn-N@C-1, and the substituents with different properties of pollutants could also cause selective oxidation. From Table S1, BA and NB had typical electron-withdrawing groups (carboxyl and nitro groups), 4-CP, BPA, 2,4-DCP, phenol had typical electron-donating groups (hydroxyl and amide groups), 2,4-DCP and phenol could be rapidly oxidized, indicating that pollutants containing electron-donating groups were more easily degraded by the Mn-N@C-1/PMS system.² It had also been reported before that $^1\text{O}_2$ could selectively oxidize organic pollutants with electron-donating groups as substrates, which further proved that the main ROS in the Mn-N@C-1/PMS system was $^1\text{O}_2$.¹

Text S4. Kinetics calculation

The competition kinetics experiment was performed using the mixed system containing nitrobenzene (NB), benzoic acid (BA), and phenol. Based on the second-order rate constants (Table S3), the steady-state concentrations of $\cdot\text{OH}$ were calculated using NB, because NB primarily reacts with $\cdot\text{OH}$, while the reaction with $\text{SO}_4^{\cdot-}$ would be negligible. Similarly, the steady-state concentrations of $\text{SO}_4^{\cdot-}$ were calculated using BA as the probe.

Table S1. Physicochemical properties of target contaminants.

Compound	Structure	MW ^a (g/mol)
2,4-Dichlorophenol		163.00
p-chlorophenol		128.56
Benzoic Acid		122.12
Nitrobenzene		123.11
p-Hydroxybenzoic acid		138.13
Phenol		94.11

^a MW: molecular weight, g/mol.

Table S2. HPLC conditions for the analysis of target contaminants.

Organics	Eluent	Flow rate (mL·min ⁻¹)	λ (nm)
2,4-Dichlorophenol	70% methanol + 30% acetic acid (0.1%)	1.0	280
p-chlorophenol	70% acetonitrile + 30% water	0.8	280
Benzoic Acid	75% methanol + 15% phosphoric acid + 10% water	0.8	230
Nitrobenzene	55% methanol + 45% water	1.0	260
p-Hydroxybenzoic acid	40% methanol + 60% acetic acid (0.3%)	1.0	270
Phenol	60% methanol + 40% phosphoric acid (0.1%)	0.8	220

Table S3. Second-order rate constants (M⁻¹ s⁻¹) between radicals and probe compounds

Compound	•OH	SO ₄ • ⁻
Nitrobenzene (NB)	4.7×10^9 ³	$< 10^6$ ⁴
Benzoic acid (BA)	2.1×10^9 ⁵	1.2×10^9 ⁶
Phenol	4.7×10^9 ⁷	2.1×10^9 ⁸

Table S4. The surface chemistry of Fresh/Used Mn-N@C-1 according to XPS results.

Sample	C (at %)	N (at %)	O (at%)	Mn (at%)
Fresh/Mn-N@C-1	77.14	14.71	5.87	2.28
Used/Mn-N@C-1	78.16	9.51	11.14	1.19

Table S5. The chemical compositions of Fresh/Used Mn-N@C-1 according to XPS results

Samples	Fresh/Mn-N@C-1	Used/Mn-N@C-1
Pyridinic N (at. %)	4.98	3.54
Pyrrolic N (at. %)	1.88	2.01
Graphitic N (at. %)	4.97	2.61
Mn-N _x (at. %)	1.87	1.13

Table S6. Characteristics of SW and ST samples.

Sample	pH	TOC (mg/L)
SW	6.5	6.74
ST	6.2	6.17

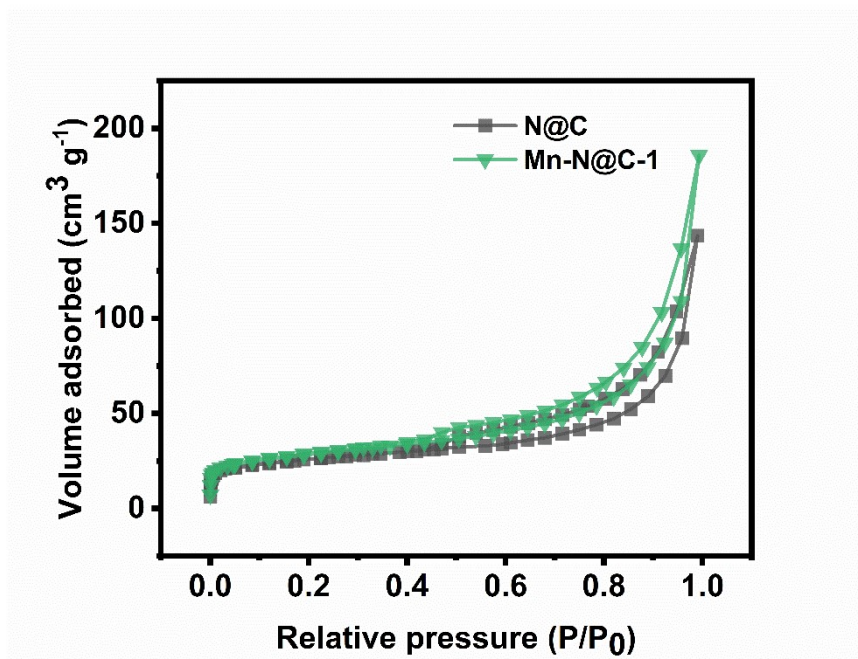


Fig. S1. N₂ adsorption–desorption isotherms of N@C and Mn-N@C-1

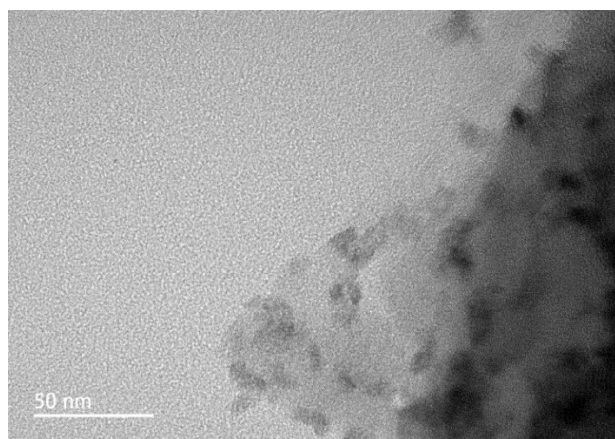


Fig. S2. TEM images of Mn-N@C-2.

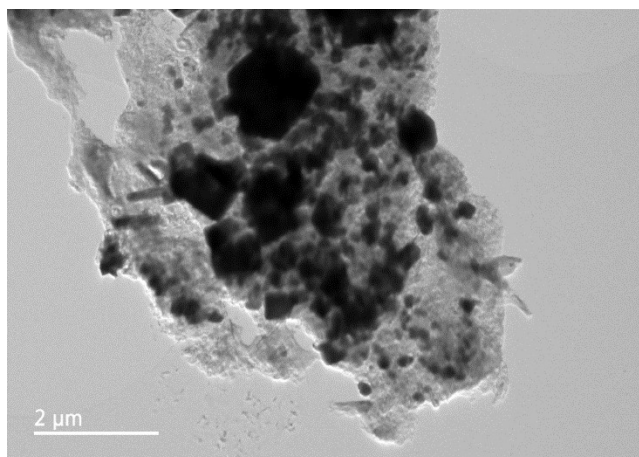


Fig. S3. TEM images of Mn@C.

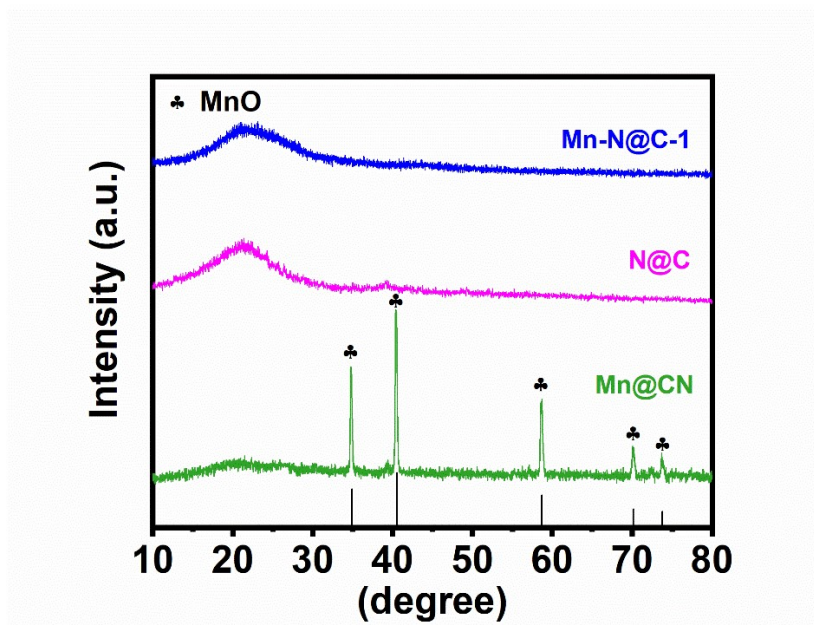


Fig. S4. XRD patterns of N@C, Mn@CN, and Mn-N@C-1.

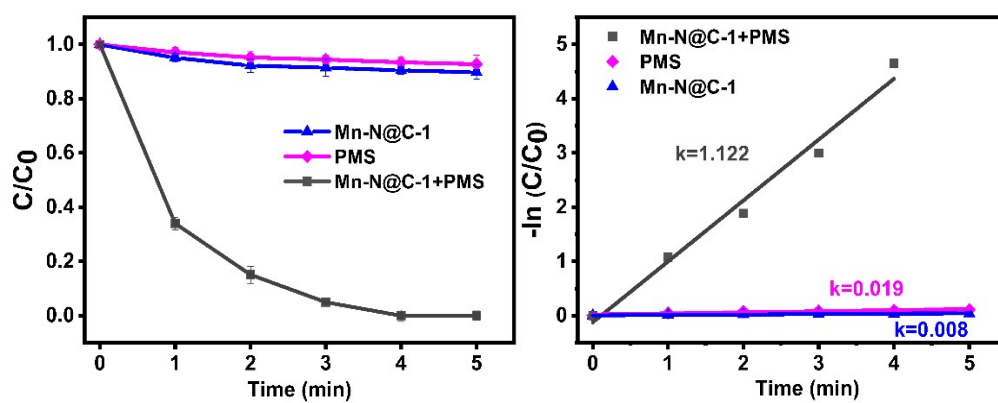


Fig. S5. (a) Phenol adsorption and oxidation of Mn-N@C-1; (b) Pseudo-first-order kinetic fitting of Mn-N@C-1 on phenol degradation. ($[\text{phenol}] = 0.2\text{g/L}$, $[\text{PMS}] = 0.2\text{ g/L}$, $[\text{catalysts}] = 0.2\text{ g/L}$, $\text{pH} = 7.0$ and room temperature).

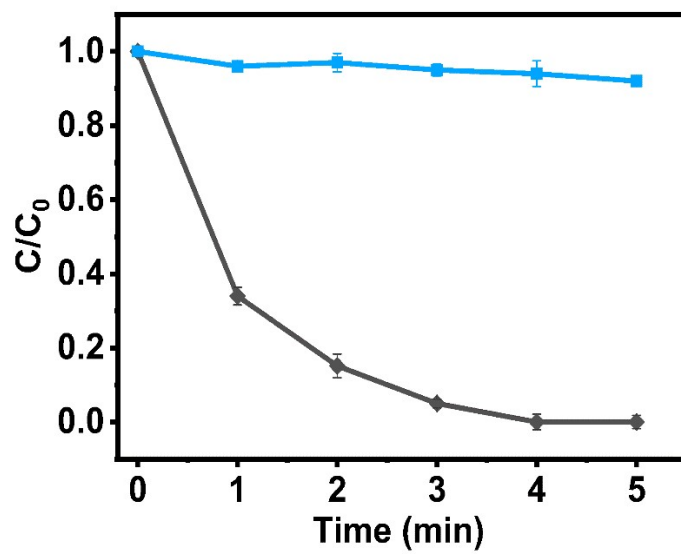


Fig. S6. Phenol oxidation of Mn@CN and Mn-N@C-1.

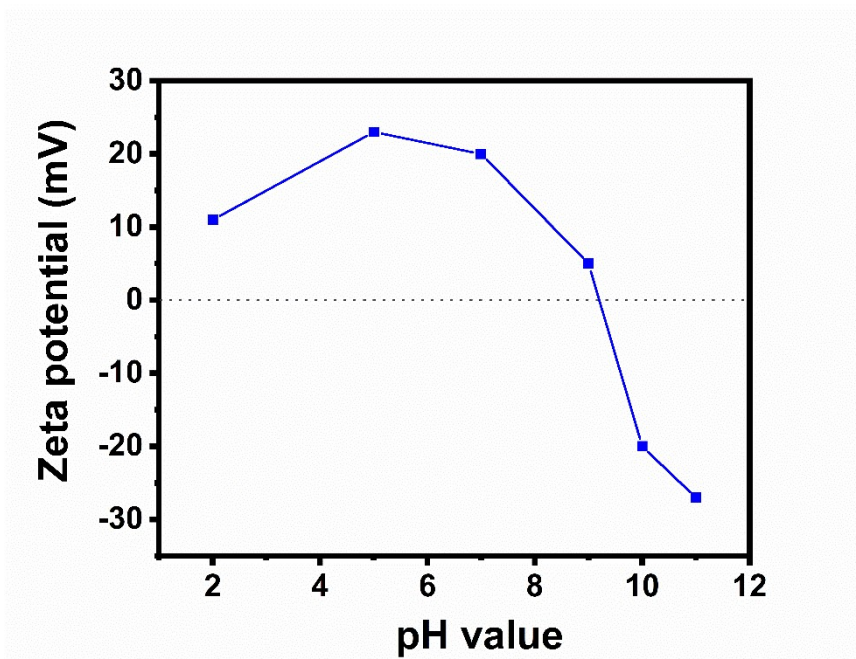


Fig. S7. Zeta potential of Mn-N@C-1

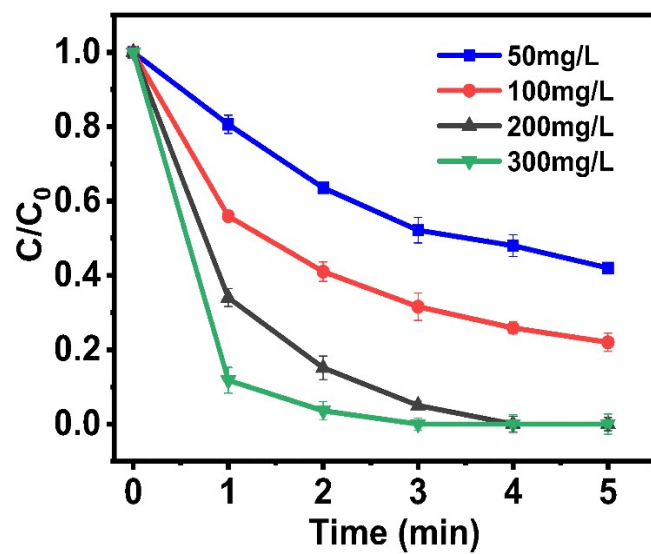


Fig. S8. Phenol degradation in Mn-N@C-1/PMS system under different Mn-N@C-1 dosage.

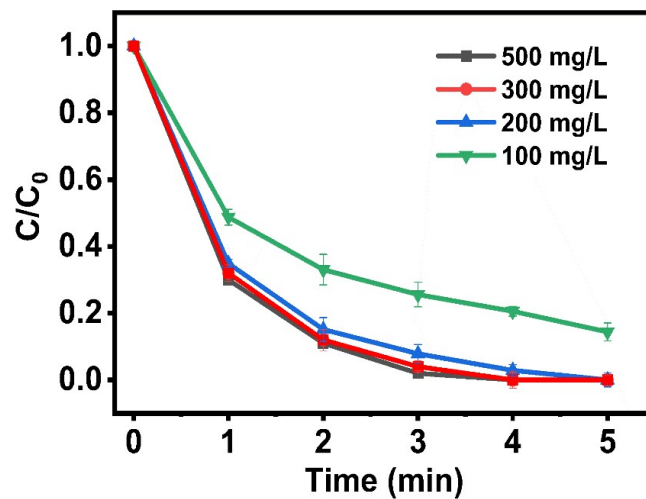


Fig. S9. Phenol degradation in Mn-N@C-1/PMS system under different PMS dosage.

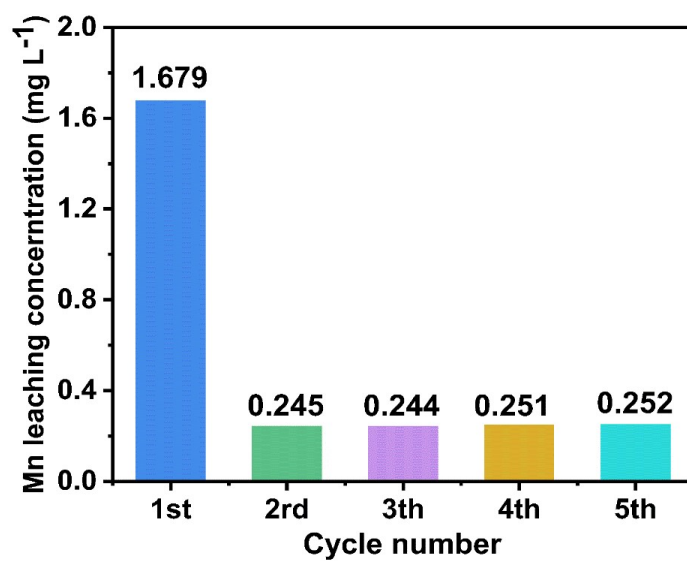


Fig. S10. The Mn leaching concentration after successive runs of phenol oxidation ([phenol] = 0.2g/L, [PMS] = 0.2 g/L, [catalysts] = 0.2 g/L, pH = 7.0 and room temperature).

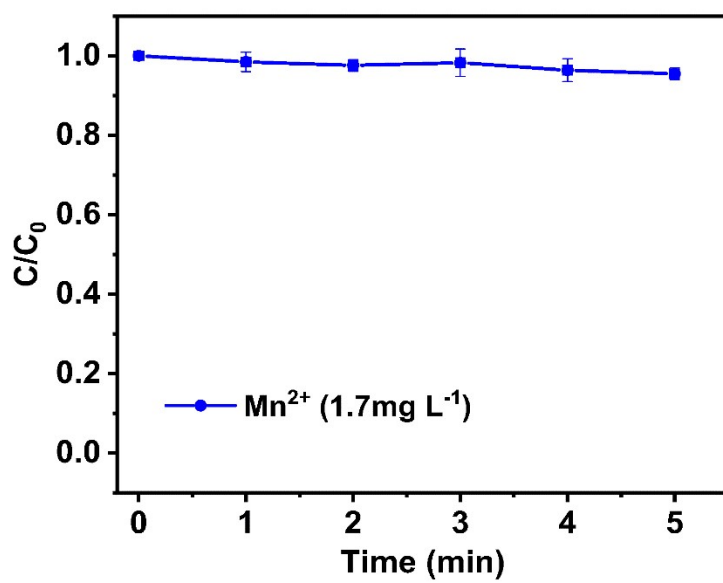


Fig. S11. Phenol degradation via PMS activation using Mn²⁺ catalyst.

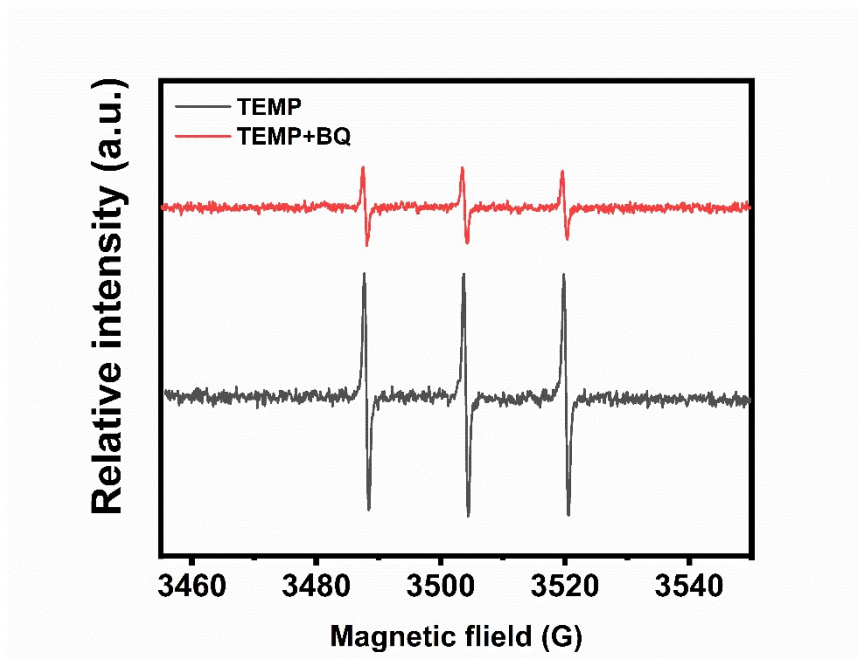


Fig. S12. EPR spectra of $^1\text{O}_2$ detection in the presence of TEMP and BQ ([PMS] = 0.2 g/L, [catalysts] = 0.2 g/L, [TEMP] = 0.35M, [BQ] = 2 mM).

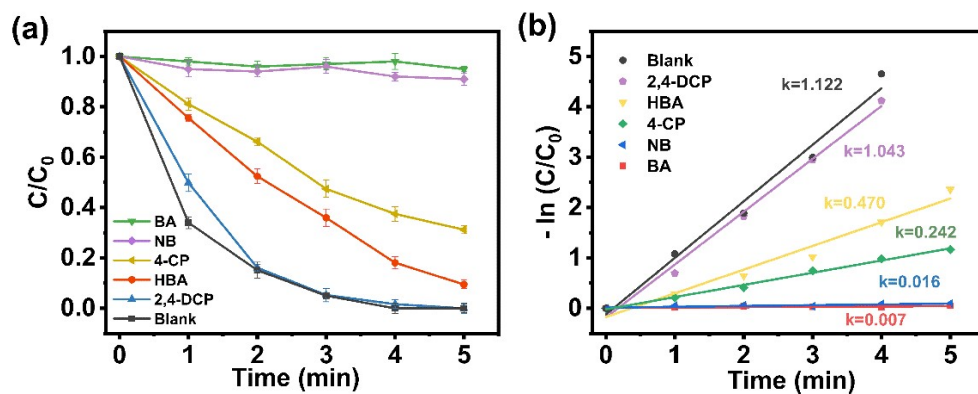


Fig. S13. (a) Selective oxidation in Mn-N@C-1/PMS system; (b) Pseudo-first-order kinetic fitting of selective oxidation in Mn-N@C-1/PMS system. ($[\text{phenol}] = 0.2\text{g/L}$, $[\text{PMS}] = 0.2\text{g/L}$, $[\text{catalysts}] = 0.2\text{g/L}$, $\text{pH} = 7.0$ and room temperature).

References

- 1 S. Zhu, X. Li, J. Kang, X. Duan and S. Wang, *Environ. Sci. Technol.*, 2019, **53**, 307-315.
- 2 X. Duan, H. Sun and S. Wang, *Acc. Chem. Res.*, 2018, **51**, 678-687.
- 3 K. D. Asmus, B. Cercek, M. Ebert, A. Henglein and A. Wigger, *Trans. Faraday Soc.*, 1967, **63**, 2435-2441.
- 4 C. Liang and H. W. Su, *Ind. Eng. Chem. Res.*, 2009, **48**, 5558-5562.
- 5 L. M. Dorfman, I. A. Taub and D. A. Harter, *J. Chem. Phys.*, 1964, **41**, 2954-2955.
- 6 P. Neta, V. Madhavan, H. Zemel and R. W. Fessenden, *J. Am. Chem. Soc.*, 1977, **99**, 163-164.
- 7 J. Bonin, I. Janik, D. Janik and D. M. Bartels, *J. Phys. Chem. A*, 2007, **111**, 1869-1878.
- 8 L. Wojnárovits and E. Takács, *Chemosphere*, 2019, **220**, 1014-1032.